Impact of turbulence anisotropy near walls in room airflow

Schälin, A.; Nielsen, Peter Vilhelm

Published in:
Indoor Air

Publication date:
2004

Document Version
Early version, also known as pre-print

Indoor Air 2004
www.blackwellpublishing.com/ina

INDOOR AIR
doi:10.1111/j.1600-0668.2004.00201.x

Impact of turbulence anisotropy near walls in room airflow

Abstract The influence of different turbulence models used in computational fluid dynamics predictions is studied in connection with room air movement. The turbulence models used are the high Re-number k–ε model and the high Re-number Reynolds stress model (RSM). The three-dimensional wall jet is selected for the work. The growth rate parallel to the wall in a three-dimensional wall jet is large compared with the growth rate perpendicular to the wall, and it is large compared with the growth rate in a free circular jet. It is shown that it is not possible to predict the high growth rate parallel with a surface in a three-dimensional wall jet by the k–ε turbulence model. Furthermore, it is shown that the growth rate can be predicted to a certain extent by the RSM with wall reflection terms. The flow in a deep room can be strongly influenced by details as the growth rate of a three-dimensional wall jet. Predictions by a k–ε model and RSM show large deviations in the occupied zone. Measurements and observations of streamline patterns in model experiments indicate that a reasonable solution is obtained by the RSM compared with the solution obtained by the k–ε model.

A. Schälin[1], P. V. Nielsen[2]
[1]Air Flow Consulting, Zürich, Switzerland, [2]Aalborg University, Aalborg, and International Centre for Indoor Environment and Energy, Technical University of Denmark, Copenhagen, Denmark

Key words: Computational fluid dynamics; Turbulence model; k–ε model; Reynolds stress model; Room air distribution; Three-dimensional wall jet; Growth rate in jet.

P. V. Nielsen
Aalborg University, Sohngaardsholmsvej 57,
DK-9000 Aalborg, Denmark
Tel.: +45 9635 8536
Fax: +45 9814 8243
e-mail: pvn@bt.aau.dk

Received for review 20 December 2001. Accepted for publication 20 February 2003.

Practical Implications
Computational fluid dynamics (CFD) is often used for the prediction of air distribution in rooms and for the evaluation of thermal comfort and indoor air quality. The most used turbulence model in CFD is the k–ε model. This model often produces good results; however, some cases require more sophisticated models. The prediction of a three-dimensional wall jet is improved if it is made by a Reynolds stress model (RSM). This model improves the prediction of the velocity level in the jet and in some special cases it may influence the entire flow in the occupied zone.

Introduction

Computational fluid dynamics (CFD) is often used for the prediction of air distribution in rooms. It is necessary to use a turbulence model in addition to the basic Navier–Stokes equation for the numerical simulation of fluid flow as the full flow simulation made by the so-called 'Direct Numerical Simulation' method would require far too much computational resources. The most frequent approach of Reynolds averaging of the governing equations with instantaneous variables is to split into mean values and fluctuating quantities, e.g. for the velocity component $\hat{u} = u + u'$, which is also expressed as a filtering with respect to time. These models are called Reynolds-averaged Navier–Stokes (RANS) models. First order RANS models include the k–ε model, second order RANS models include the Reynolds stress model (RSM). Large-eddy simulation represents an alternative approach where the variables are filtered with respect to grid space.

The k–ε turbulence model is based on two transport equations, one for turbulent kinetic energy and one for dissipation of turbulent kinetic energy, and it is most widely used in all engineering applications including room ventilation. This model was developed for fully turbulent channel flow and is well known to give good predictions in many situations but also known to show some deficiencies in some types of flows, which limits the accuracy for general applications. Much development is therefore continually made as modifications of the k–ε model or as a development of more advanced turbulence models such as the RSM turbulence models in order to overcome prediction problems in certain situations. (For modification of the k–ε model in predictions of room air distribution see Nielsen, 1998a.)

An important limitation of the k–ε model is the assumption of turbulence isotropy. This model solves the turbulent kinetic energy $k = 1/2(\overline{u'^2} + \overline{v'^2} + \overline{w'^2})$ where u', v' and w' are the fluctuating velocity components, and it solves the dissipation rate ε of the

turbulent kinetic energy. The components u', v' and w' are obviously treated equally. Individual influences of the fluctuating quantities on the flow are, however, quite important in several types of flows. Such effects are taken into account in anisotropic turbulence models as higher order RANS models like the RSM. Second order correlations of u', v', w' as $\overline{u'^2}$,..., $\overline{u'v'}$... represent anisotropy and they are discussed in the RSM. The equations in RSM require further modeling for closure as even higher order terms appear in the equations. Examples of flows where anisotropy plays an important role are swirling flow, stress-driven secondary flow and near-wall flow.

The paper deals with three-dimensional wall jets that are found frequently in ventilated rooms with high velocity air terminal devices and mixing ventilation. It is known that the growth rate parallel to surfaces is too small when the k–ε model is used. The shortcomings of the k–ε model as regards near wall flow were obvious in some very early CFD predictions of three-dimensional flow (Gosman et al., 1980). New predictions with a low-Re k–ε model show the same shortcomings in the prediction of growth rates in a three-dimensional wall jet (Davidson and Nielsen, 2003). Measurements made by Blum (1956), show a large growth in the three-dimensional wall jet width parallel to the wall and a much smaller growth in width perpendicular to the wall. Predictions by a k–ε model show an identical growth rate in both directions. The problem was partly overcome by the use of the so-called prescribed velocity method (Nielsen, 1992, 1998b) where the wall jet is prescribed in a volume in front of the supply opening and, therefore, suppresses the effect in this part of the jet flow. The main idea behind the prescribed velocity method is to reduce the number of grid cells by prescribing the flow from the diffuser without working with the details of the geometry and flow in an actual diffuser.

The reason of failure of the k–ε model in the three-dimensional wall jet predictions can be ascribed to the fact that the damping of the turbulence fluctuations perpendicular to the wall, an anisotropy effect, is inherently absent in the k–ε model.

This paper shows new prediction improvements for the case (Blum, 1956) by the use of RSM. The model does not impose on certain knowledge of the experimental values in the prediction area as in the prescribed velocity method, and is therefore better suited for the application both close to the air terminal device and in the whole flow regime.

The application of the RSM is also shown in another situation where the use of the k–ε model strongly fails, namely in the case of flow with an isothermal three-dimensional wall jet in a very long room. In this case, the predictions of the wall jet properties are different from the experiments. The experiments show asymmetrical flow behaviour, even for symmetrical boundary conditions, and this special flow feature can be captured by using the RSM instead of the k–ε model. Such asymmetrical flow effects under symmetrical boundary conditions are known to occur in certain other situations (e.g. Bjerg et al., 1999), but they will often disappear if the room is short.

Turbulence models

The CFD simulations have been made by the use of a Fluent code. The turbulence models applied are the standard high-Re k–ε model and the high-Re RSM model with options implemented in the Fluent code. The options relevant in the application presented here are the so-called wall reflection terms following the standard RSM approach described by Launder (1989a).

The k–ε model is a two-equation model based on both a transport equation for turbulent kinetic energy k and a transport equation for the dissipation of turbulent kinetic energy ε (Launder and Spalding, 1974).

A general formulation is given by Equations 1–3

$$\frac{D\rho k}{Dt} = D_k + P_k + G_k - \rho\varepsilon \tag{1}$$

$$\frac{D\rho\varepsilon}{Dt} = D_\varepsilon + C_1\frac{\varepsilon}{k}(P_k + C_3G_k) - C_2\rho\frac{\varepsilon^2}{k} \tag{2}$$

The turbulent viscosity μ_t is obtained from

$$\mu_t = \rho C_\mu \frac{k^2}{\varepsilon} \tag{3}$$

D_k, P_k and G_k are diffusion, production and buoyancy terms in the k equation and D_ε is the diffusion term in the ε equation. ρ is density and C_1, C_2, C_3 and C_μ are universal constants in the k–ε model.

The RSM is a seven-equation model. The Reynolds stress transport equations are modeled in the following form:

$$\frac{D\left(\rho\overline{u_i'u_j'}\right)}{Dt} = D_{ij}^T + D_{ij}^L + P_{ij} + G_{ij} + \phi_{ij} - \varepsilon_{ij} + F_{ij} \tag{4}$$

D_{ij}^{T}, D_{ij}^{L}, P_{ij}, G_{ij}, F_{ij} and ϕ_{ij} are turbulent diffusion, molecular diffusion, stress production, buoyancy production, production by system rotation and pressure strain terms. ε_{ij} is the dissipation tensor. The dissipation equation (2) is solved together with the six Reynolds stress equations and the stresses $\rho\overline{u_i'u_j'}$ describe the turbulence in the RANS equations.

The k–ε model solves the turbulence as a distribution of turbulent viscosity μ_t. It is not possible to consider anisotropic effect in the flow, and the normal stresses are only expressed on an average by

$$k = \frac{1}{2}\rho\overline{u_i' u_i'} \tag{5}$$

The RSM gives all six Reynolds stresses $\rho\overline{u_i' u_j'}$ and it is clearly superior in situations where the anisotropy of turbulence has a dominant effect on the mean flow. Such cases include highly swirling flows and stress-driven secondary flows. Equation 4 is given in details in Appendix A.

The pressure-strain term ϕ_{ij} in Equation 4 can be developed in a linear-strain model as

$$\phi_{ij} = \phi_{ij,1} + \phi_{ij,2} + \phi_{ij}^{w} \tag{6}$$

where $\phi_{ij,1}$ and $\phi_{ij,2}$ are called the 'slow pressure-strain' terms and the 'rapid pressure-strain' terms. ϕ_{ij}^{w} are the 'wall-reflection' terms. Equation 6 is given in details in Appendix B.

The wall reflection terms are responsible for the redistribution of normal stresses near the wall. They damp the turbulent fluctuations perpendicular to the wall and convert the energy to the fluctuations parallel to the wall. The calculated jet widths perpendicular to the wall will be smaller and the calculated jet widths parallel to the walls become wider, which is identical to the behaviour in a real wall jet when the flow is predicted by RSM.

RSM without the wall reflection terms as well as other turbulence models like the k–ε model is not able to take this effect into account, although it is very important for the prediction of room air distribution as shown in this paper.

The wall reflection terms explained so far have also application limits. They are valid for flows parallel to the wall but not for impinging flows or for the presence of additional walls in full three-dimensional room configurations. Craft et al. (1993) suggested modified expressions for the pressure-strain terms to represent these effects but they have not been applied in the present study. A thorough discussion of the redistribution processes is given by Launder (1989a) or Jakirlic (1997).

Overview of the cases

The airflow in rooms with a three-dimensional wall jet has been investigated and analyzed in a large number of cases, from which two cases that exhibit particularly interesting effects have been selected. The presented cases are isothermal cases and they cover comparisons between measurements and numerical predictions by use of k–ε and RSM turbulence models. The two cases deal with a short room and a long (deep) room, respectively.

All the predictions are made by the commercial code: Fluent 5.4.8. The discretization scheme used is of second order accuracy with a second order upwind scheme for the convection terms. The equations are solved by the SIMPLE algorithm. The geometry is fairly simple with flow parallel to grid lines close to the supply opening. It is possible to demonstrate a grid-independent solution for a grid with 17,280 cells. (The predictions are compared with solutions obtained in a grid of 75,330 cells.) The range of y^+ in the wall function is 20–40 in the wall jet regions in all cases.

Both the high-Re k–ε model and the high-Re RSM are used with wall functions.

The short room case was investigated in 1956 by Blum and the measurements can be found in Gosman et al. (1980). Figure 1 shows the set-up of the test case with a circular inlet nozzle (height, H; width, W; length, L; inlet nozzle diameter, d).

The parameters are as follows:

Dimensions: $H = 1.0$ m, $d/H = 0.04$, $W/H = 1.0$, $L/H = 3$, $t/H = 0.03$

Flow parameters: $Re = 90{,}000$ based on d (inlet velocity 35 m/s).

The long room case was investigated by Nielsen (1974). Figure 2 shows the set-up of this test case (height, H; width, W; length, L; slot inlet nozzle: height, h; width, w).

The parameters are as follows:

Dimensions: $H = 0.128$ m, $h/H = 0.025$, $W/H = 4.7$, $w/W = 0.2$, $L/H = 12$, $t/H = 0.16$

Flow parameters: $Re = 4700$ based on h (inlet velocity 22.4 m/s).

The original measurements have been reproduced in a similar configuration in Jensen (2000):

Dimensions: $H = 0.0714$ m, $h/H = 0.056$, $W/H = 5.0$, $w/W = 0.2$, $L/H = 14$

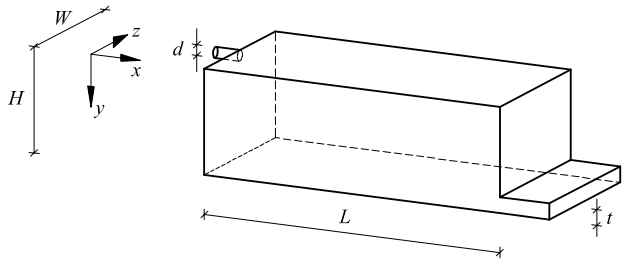

Fig. 1 The geometry of the short experimental chamber (Blum, 1956) with a length-to-height ratio $L/H = 3$

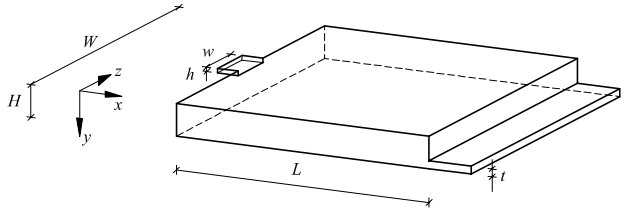

Fig. 2 The geometry of the long experimental chamber (Nielsen, 1974) with a length-to-height ratio $L/H = 12$

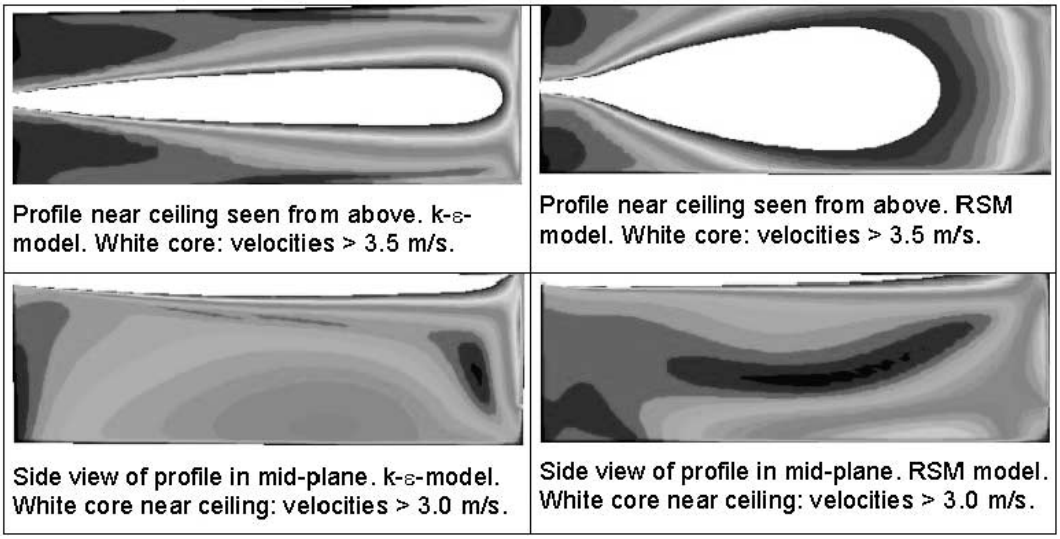

Fig. 3 CFD prediction of the velocity distribution in the short room. Inlet velocity 35 m/s

Flow parameters: $Re = 4000$ based on h (inlet velocity 15.1 m/s).

Results for the short room

In the short room case the attention is directed towards the detailed comparison of the three-dimensional wall jet itself. Figure 3 shows the predicted flow of the wall jets in the short room configuration. The k–ε model produces a thick and narrow jet, whereas RSM produces a wider jet, which leads to lower velocities also in the lower part of the room when the airflow bends back to the inlet plane along the floor. Like the experiments all predictions are made with a circular inlet nozzle.

Figure 4 shows the detailed evaluation of the profiles along the wall jet below the ceiling. The profiles at a certain distance x along the length of the chamber are defined by the distance δ_y from the ceiling to the normal (y) location where the velocity has decreased by 50% and by the distance δ_z from the symmetry plane to the lateral (z) location where the velocity in the profile has decreased by 50%, respectively, as shown in Figure 4a. u_o is the jet velocity at the nozzle. The other values are defined in Figure 4a.

Figure 4b shows the decay of the center line peak velocity, which is predicted very well by RSM compared with the results obtained by the k–ε model. There are small deviations in the RSM model predictions (about 10%) towards the end of the chamber but the k–ε model values are 50–80% too high.

Figure 4c shows the normal profile widths and Figure 4d the lateral profile width. The normal profile widths (indicating the normal 'thickness' of the jet) predicted by RSM are a little too small, the slope, however, fits well with the experimental wall jet. The experimental growth rate D_y is 0.048, and the growth rate found by predictions made by the RSM is 0.047. The growth rate D_y is equal to 0.047 for the predictions made by the k–ε model, slightly below the findings in Davidson and Nielsen (2003) with a low-Re k–ε model. D_y is given from

$$\delta_y = D_y\left(x + x_{o,y}\right) \tag{7}$$

where $x_{o,y}$ is the virtual origin of the wall jet with respect to the normal profile. The virtual origin is the location where the line $\delta_y(x)$ is crossing the x-axis. The fact that the profile widths in this case do not match exactly the measured profiles is probably related to the fact that the lateral distribution of the jet in the second part of the chamber is predicted to a level that is too high.

The k–ε model seems to perform better when looking at Figure 4c, but the chosen evaluation is somewhat misleading. A closer look at the predictions made by the k–ε model shows a broad tail in the velocity profiles, which is not present at that level in the RSM predictions.

The lateral profile widths (indicating the 'broadness' of the jet) predicted by RSM fit very well in the first part of the jet. The experimental growth rate D_z is 0.23 and the growth rate found by predictions made by the RSM is 0.27. The growth rate D_z is equal to 0.07 for the predictions made by the k–ε model corresponding to the findings in Davidson and Nielsen (2003) with a low-Re k–ε model. D_z is given from

$$\delta_z = D_z(x + x_{o,z})$$

where $x_{o,z}$ is the virtual origin of the wall jet connected to the lateral profile. In the second part of the chamber the jet attaches itself too strong to the side wall. This might be related to the known and mentioned

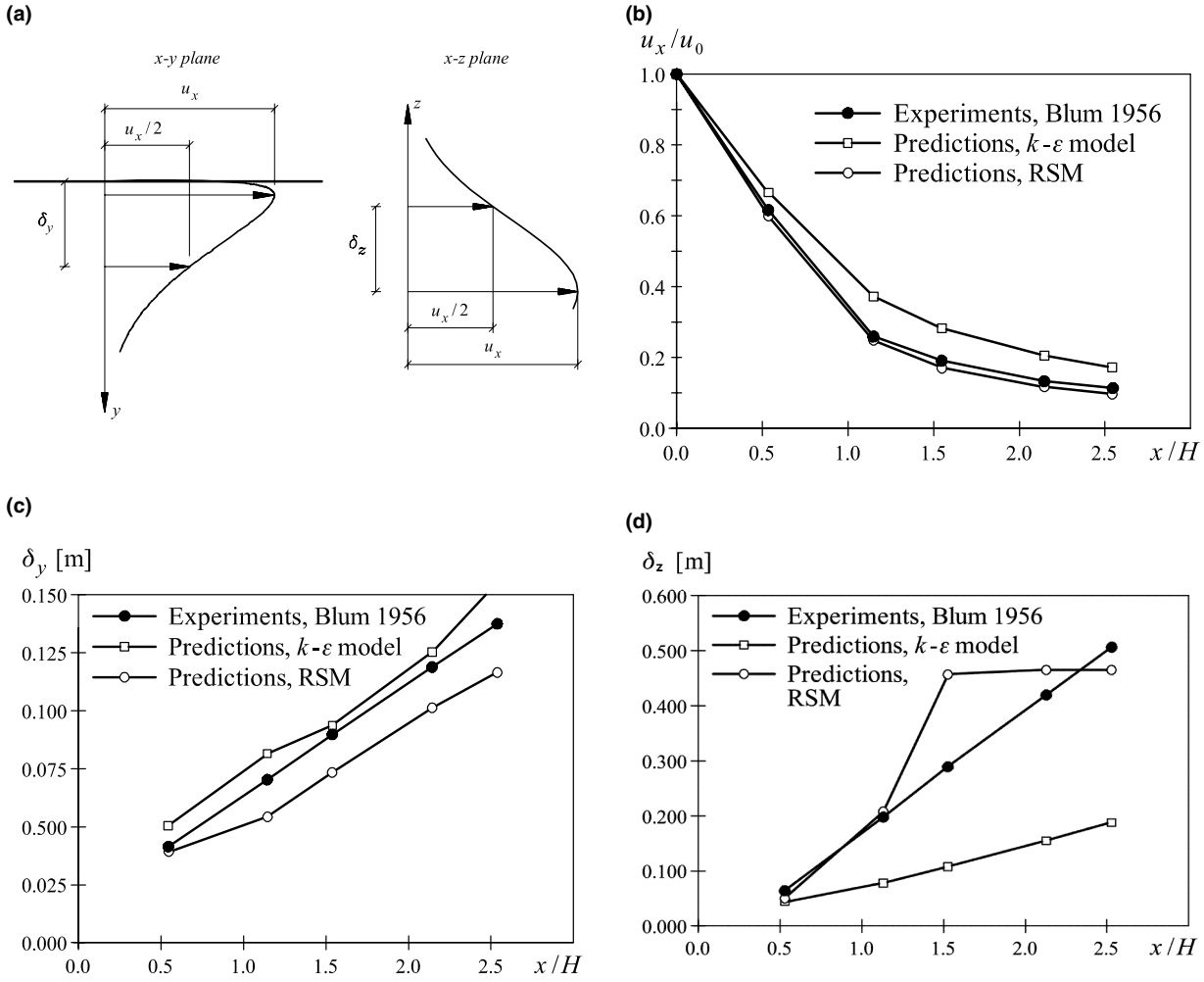

Fig. 4 (a) Sketch of a wall jet and definition of u_x, δ_y and δ_z. (b) Comparison between experiments and CFD for Blum's (1956) configuration. Decay of center line peak velocity. (c) Comparison between experiments and CFD for Blum's (1956) configuration. Normal profile width vs. distance. (d) Comparison between experiments and CFD for Blum's (1956) configuration. Lateral profile width vs. distance

limitation of the used wall reflection terms. They are applicable for parallel flow along a wall but not optimal for an impinging flow at the end of the room or for the presence of additional side walls in a three-dimensional geometry as it is the case in the present situation. The neighbourhood of the side walls might cause a too high drawing of turbulent energy to the sides. In this case this effect seems to be responsible for the overestimated width of the wall jet. The effect is not very strong but the evaluated quantities are in this case strongly dependent on these deviations.

The prediction of the wall jet is considerably better when the RSM model is used, even if the presence of the side walls leads to a too strong increase of jet width.

Results for the long room

In the long room, attention is focused on the general flow pattern in the whole room. The observation of the air movement in the room showed a horizontal rotating movement close to the floor in the full width of the model below the supply opening. Figure 5a shows the visualized airflow using metaldehyde particles (from Nielsen, 1974). The accumulation of rotating particles below the supply opening is clearly visible in the photograph. It was concluded that this air movement was a result of a slightly asymmetrical flow in the supply jet in the upper part of the model. The jet was partly displaced to one side in the deep model and the return flow in the lower part of the model was therefore concentrated in the opposite side of the model. Figure 5b shows a sketch of this air movement from Nielsen (1974).

There have not been any measurements in the experiments made in 1974 except the observations described and, therefore, it was not possible to decide the degree of asymmetrical flow except the fact that it has the strength to generate a horizontal rotating flow with a diameter of W in the lower part of the model close to the supply end wall.

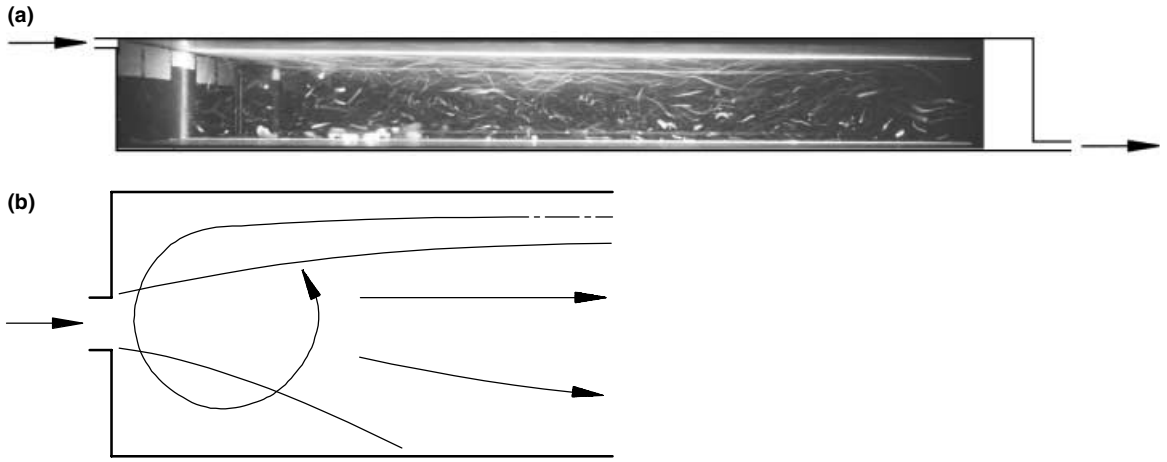

Fig. 5 Flow in a long room. (a) Flow seen in symmetry plane from the side. Accumulation of rotating particles below supply. (b) Sketch of flow (Nielsen, 1974)

The original measurements have been reproduced in a similar configuration in Jensen (2000) and have been evaluated in a more quantitative way. Figure 6 shows velocity profiles along several lines perpendicular to the main flow direction close to the ceiling and the floor. The inlet jet is not tilted intentionally. The results in Figure 6 show again the tendency of the jet to turn in a slightly asymmetrical way to one corner, which finally leads the return flow along the floor to a highly enhanced asymmetrical flow towards the opposite corner.

The k–ε model and the RSM have been used in the predictions and the boundary conditions have been varied in a certain range to study their influence on the results. The results of the CFD predictions are given in the following Table 1 with an overview of the different cases and their boundary conditions. The different boundary conditions include:

- Lateral velocity component w_o (parallel to the ceiling, corresponding to the z direction in Figure 4a). This velocity will impose a slight asymmetry on the inlet boundary condition.
- Turbulence intensity k_o and turbulence length scale ℓ_o of the inlet jet.

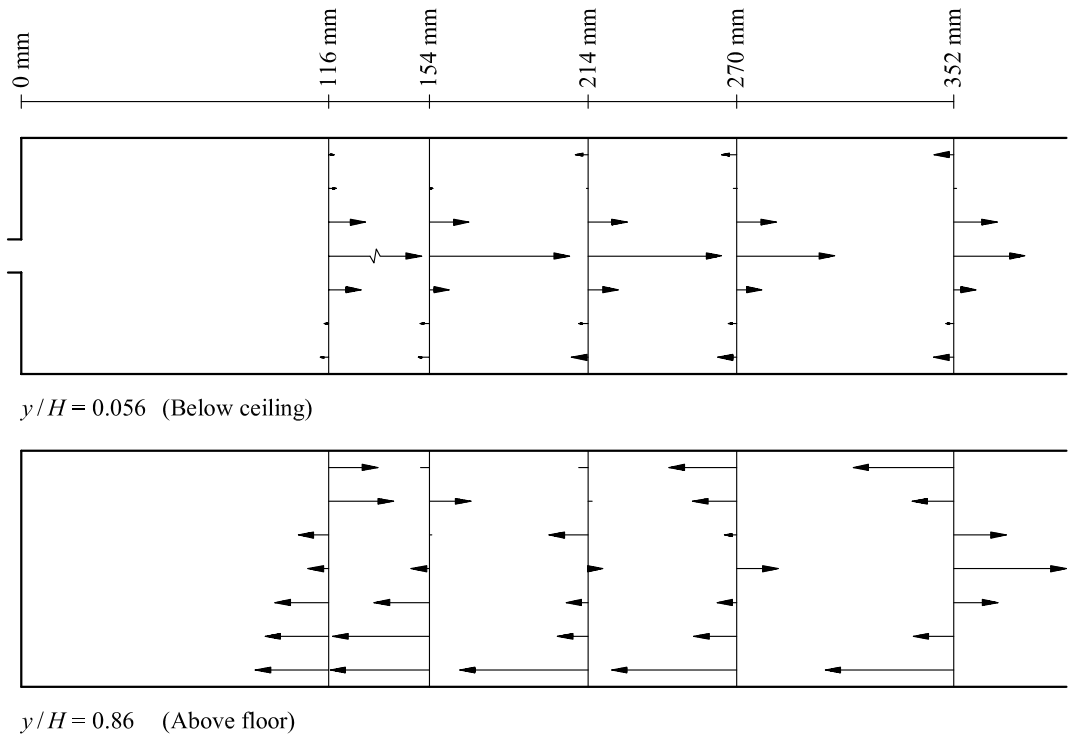

Fig. 6 Flow in the upper and lower part of a long room (Jensen, 2000). $h/H = 0.056$, $w/W = 0.2$, $L/H = 14.0$ and $W/H = 5.0$

Table 1 Overview of inlet boundary conditions. 1a, restart from 1; 1b, from initial conditions; ϕ_{ij}^{w} off, 'wall reflection terms in RSM turned off' (normally they are activated)

Name of case	Model	u_o velocity (m/s)	w_o velocity (m/s)	w_o/u_o	Inlet turbulence Tu (%)	l_o (m)	Turbulence model	Convergence
Ke-1	1	22.4	0.224	0.01	4	0.001	k–ε	Good
RSM-1	1	22.4	0.224	0.01	4	0.001	RSM, ϕ_{ij}^{w} on	Good
RSM-1a,b	1	22.4	0.045	0.002	4	0.001	RSM, ϕ_{ij}^{w} on	Medium
RSM-1c	1	22.4	0.0	0	4	0.001	RSM, ϕ_{ij}^{w} on	Poor
RSM-1d	1	22.4	0.045	0.002	0.1	0.0001	RSM, ϕ_{ij}^{w} on	Medium
RSM-1e	1	22.4	0.045	0.002	15	0.02	RSM, ϕ_{ij}^{w} on	Poor
RSM-1f	1	22.4	0.045	0.002	4	0.001	RSM, ϕ_{ij}^{w} off	Poor
RSM-2	2	22.4	0.045	0.002	4	0.001	RSM, ϕ_{ij}^{w} on	Not so good

The reason for the slight asymmetry in the boundary conditions is to find out how much asymmetry is necessary (if any at all) to produce an asymmetrical flow pattern as the one observed experimentally.

The normal component is always $u_o = 22.4$ m/s and the lateral component parallel to the ceiling varied from $w_o = 0$ to $w_o = 0.1 \times u_o$ (corresponds to an exit angle of 5.7°); usually the tilt angle is very small (0.57° for $v_o = 0.01 \times u_o$ and 0.11° for $v_o = 0.002 \times u_o$).

There were two models applied with two sizes of grid cells to check for grid independence of the results.

Model 1: 17,280 grid cells, 24 across L, 40 across W, 18 across H, 11×6 across the inlet.

Model 2: 75,330 grid cells, approximately 1.63^3 times more cells,

45 across L, 62 across W, 27 across H, 18×9 across the inlet.

The numerical parameter study revealed a number of remarkable features:

- For symmetrical boundary conditions the results found by the k–ε model are symmetrical in cases where the room has a width to height ratio $W/H \sim 5$ (in contrast to the experimental findings).
- By use of the k–ε model and an exit angle of 0.57° (Case Ke-1) the jet bends out a little more but goes back towards the normal direction with some displacement. This situation is shown in Figure 7. The flow near the floor is almost symmetrical. The cross-plane pictures show that the wall jet is spreading considerably downwards in the direction perpendicular to the ceiling.

Experience from many previous simulations has already shown that the k–ε model does not yield an asymmetrical flow pattern. Firstly, this is attributed to the fact that the normal spreading is too strong, and secondly as a consequence of the thick wall jet that the

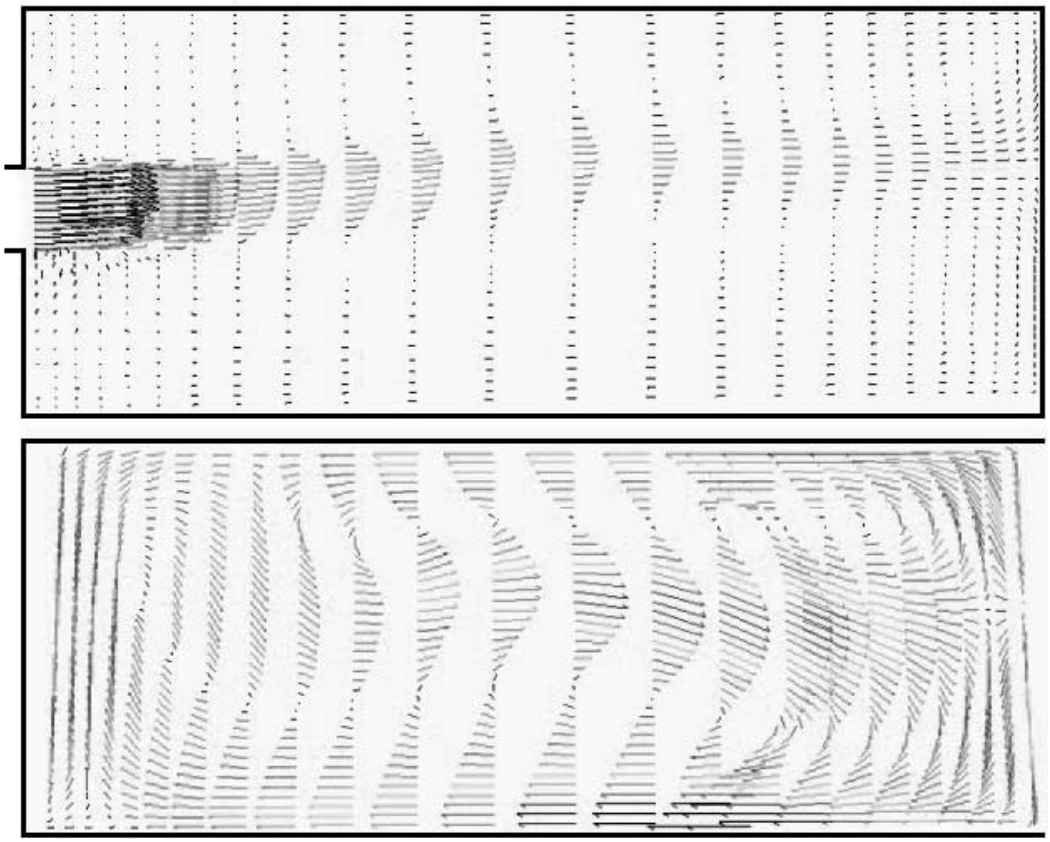

Fig. 7 CFD results for a long room $l/H = 12$ using the k–ε model. Above: Velocity contours near ceiling. Below: Vectors in plane close to the floor

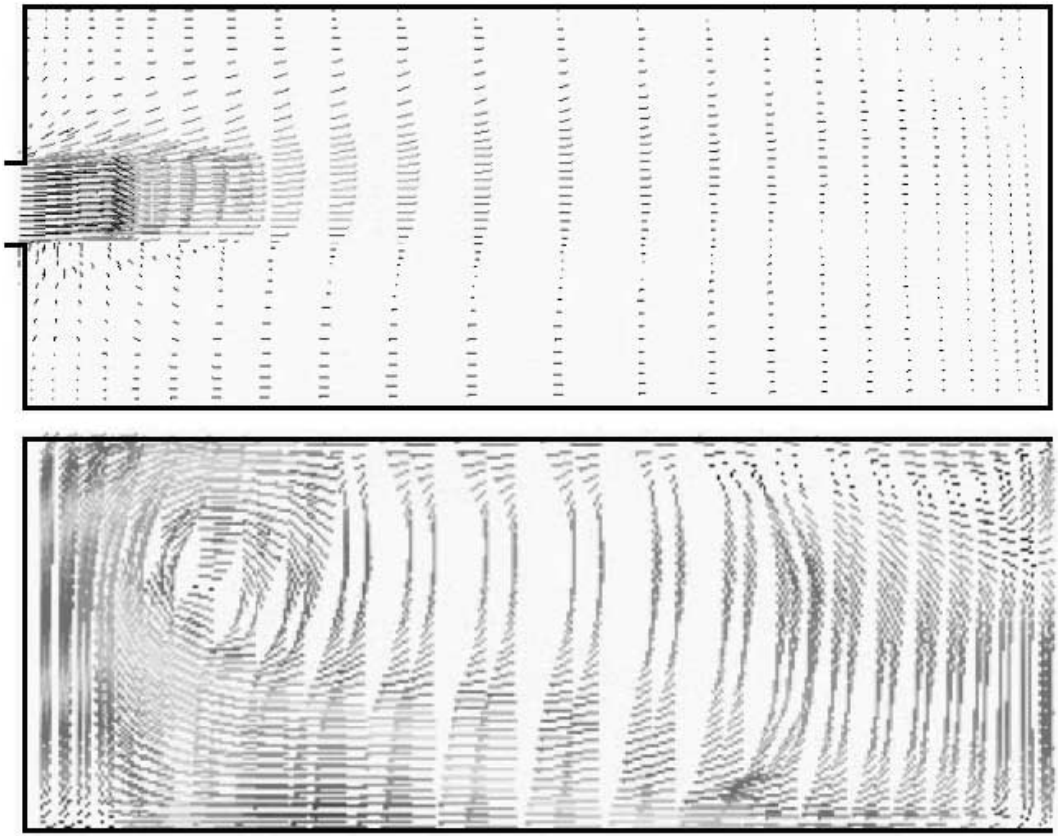

Fig. 8 CFD results for a long room $l/H = 12$ using the RSM model. Above: Velocity contours near ceiling. Below: Vectors in plane close to the floor indicating the rotating flow below the supply, similar to the experimental findings in Figures 5 and 6

return flow on both sides of the jet tends to stabilize the forward jet flow in the middle of the room independent of the initial tilt.

- By use of RSM and an exit angle of 0.57° (Case RSM-1) the jet turns more to the corner and as a consequence there is a strong swirl on the floor below the supply in a very similar way as it was found in the early 1974 experiments. This situation is shown in Figure 8.
- Also at the smaller angle of 0.11° (which is practically perpendicular) the jet tends towards the corner (Case RSM-1a or 1b). However, the convergence is better at the larger angle. It seems that the perpendicular jet with the current room aspect ratios does not have a stable solution in the symmetry plane by the use of RSM. This also corresponds to the physically observed situation.
- The simulation at an exit angle of strictly zero (Case RSM-1c) did not converge to low residual values, which supports the statement above that there is not a stable solution for this situation.
- The usual inlet turbulence is 4% and the turbulence length scale is 0.001 m (slot height 0.0032 m). A change in inlet turbulence to 0.1% (Case RSM-1d) gives the same results and a case with a turbulence intensity of 15% did not converge well (Case RSM-1e).

The cross-plane pictures of the RSM cases show again that the jet attaches much more to the ceiling than in the k–ε model case and exhibits a larger δ_z.

This feature can easily be attributed to the anisotropy effect of the wall reflection terms in the RSM turbulence model described in the model section. Because of the presence of the wall the perpendicular fluctuations are damped, which keeps the jet closer to the wall (the ceiling in the present case), and the energy is redistributed into the parallel stress terms:

- when the wall reflection terms are deactivated in the case RSM-1f the result shows a similar jet as in the k–ε case;
- the cases with higher grid resolution (Case RSM-2) lead to the same results, which proves sufficient grid resolution for the present case; the convergence behaviour, however, was not as good as in the coarser grid case.

The tendency of a jet to attach to a wall (as it is also observed here for the wall jet to attach to one side wall) as a result of unsymmetrical pressure forces, with a low pressure on the wall side, is known as the Coanda effect.

The configuration in this paper is an example of a case where a three-dimensional unsymmetrical flow pattern is obtained, although the boundary conditions indicate the possibility of a symmetrical flow. This flow situation has also been observed in other wide rooms as described by Bjerg et al. (1999).

Conclusions

The k–ε turbulence model is an acceptable model in many situations in room air movement, but this paper shows situations where the usually hidden problems clearly arise and illustrate the need and advantage of better models. The wall jet behaviour can be captured to a better degree by the use of suited wall reflection terms in RANS models, which can be included in RSM and algebraic stress models (ASM). The use of wall reflection terms also show some limitations; however, by further improvements of this model it is expected to match the experimental values even better.

Acknowledgements

The VELUX Research Programme has supported this work and the first author has stayed at Aalborg University as a VELUX Visiting Professor three times during the research period. The International Centre for Indoor Environment has supported this work with research funds for the second author.

References

Bjerg, B., Morsing, S., Svidt, K. and Zhang, G. (1999) Three-dimensional airflow in a livestock test Room with two-dimensional boundary conditions, *J. Agric. Engng. Res.*, **74**, 267–274.

Blum, W. (1956) *Diplomarbeit*, Germany, Aachen.

Craft, T.J., Graham, L.J.W. and Launder, B.E. (1993) Impinging jet studies for turbulence model assessment – II. An examination of the performance of four turbulence models, *Int. J. Heat Mass Transfer*, **36**, 2685–2697.

Davidson, L. and Nielsen, P.V. (2003) *Comparing a k–ε Model and the v^2–f Model in a 3D Isothermal Wall Jet*, Technical Report, ISSN 1395-7953 R0301, Denmark, Aalborg University.

Fu, S., Launder, B.E. and Leschziner, M.A. (1987) Modeling strongly swirling recirculating jet flow with Reynolds-stress transport closures. In: *Sixth Symposium on Turbulent Shear Flows*, France, Toulouse, 1987.

Gibson, M.M. and Launder, B.E. (1978) Ground effects on pressure fluctuations in the atmospheric boundary layer, *J. Fluid Mech.*, **86**, 491–511.

Gosman, A.D., Nielsen, P.V., Restivo, A. and Whitelaw, J.H. (1980) The flow properties of rooms with small ventilation openings, *ASME Trans.*, **102**, 316–323.

Jakirlic, S. (1997) Reynolds-Spannungs-Modellierung komplexer turbulenter Strömungen. PhD Thesis, Herbert Utz Verlag Wissenschaft, Munich, Germany.

Jensen, J.P. (2000) *Personal Communication*, Denmark, Aalborg University.

Launder, B.E. (1989a) Second-moment closure: present … and future? *Int. J. Heat Fluid Flow*, **10**, 282–300.

Launder B.E. (1989b) Second-moment closure and its use in modeling turbulent industrial flows, *Int. J. Numer. Meth. Fluids*, **9**, 963–985.

Launder, B.E. and Spalding, D.B. (1974) The computation of turbulent flows. *Comp. Meth. Appl. Mech. Eng.*, **3**, 269–289.

Lien, F.S. and Leschziner, M.A. (1994) Assessment of turbulent transport models including non-linear RNG eddy-viscosity formulation and second-moment closure, *Computers Fluids*, **23**, 983–1004.

Nielsen, P.V. (1974) Flow in air-conditioned rooms. PhD Thesis, Technical University of Denmark, Copenhagen.

Nielsen, P.V. (1992) The description of supply openings in numerical models for room air distribution, *ASHRAE Trans.*, **98**, 963–971.

Nielsen, P.V. (1998a) The selection of turbulence models for prediction of room airflow, *ASHRAE Trans.*, **104**, 1119–1127.

Nielsen, P.V. (1998b) *The Prescribed Velocity Method – A Practical Procedure for Introduction of an Air Terminal Device in CFD Calculation*. Technical Report, ISSN 1395-7953 R9827, Denmark, Aalborg University.

Sarkar, S. and Balakrishnan, L. (1990) *Application of a Reynolds-Stress Turbulence Model to the Compressible Shear Layer*. ICASE Report 90-18, NASA CR 182002.

Appendix A

The Reynolds stress transport equation is given by

$$\frac{D(\rho\overline{u_i'u_j'})}{Dt} = D_{ij}^T + D_{ij}^L + P_{ij} + G_{ij} + \phi_{ij} - \varepsilon_{ij} + F_{ij}$$

D_{ij}^L, P_{ij} and F_{ij} do not require any modeling and they are expressed by the following terms:

$$D_{ij}^L = \frac{\partial}{\partial x_k}\left[\mu\frac{\partial}{\partial x_k}(\overline{u_i'u_j'})\right]$$

$$P_{ij} = -\rho\left(\overline{u_i'u_k'}\frac{\partial u_i}{\partial x_k} + \overline{u_j'u_k'}\frac{\partial u_i}{\partial x_k}\right)$$

$$F_{ij} = -2\rho\Omega_k\left(\overline{u_j'u_m'}\varepsilon_{jkm} + \overline{u_i'u_m'}\varepsilon_{jkm}\right)$$

The terms D_{ij}^T, G_{ij} and ε_{ij} need to be modeled to close the equation system

$$D_{ij}^T = \frac{\partial}{\partial x_k}\left(\frac{\mu_t}{\sigma_k}\frac{\partial\overline{u_i'u_j'}}{\partial x_k}\right)$$

where $\sigma_k = 0.82$, (Lien and Leschziner, 1994).

The flow is isothermal and the production term due to buoyancy G_{ij} will therefore not be present in the predictions.

The dissipation tensor, ε_{ij}, is modeled as

$$\varepsilon_{ij} = \frac{2}{3}\delta_{ij}(\rho\varepsilon + Y_M)$$

where $Y_M = \rho\varepsilon 2M_t^2$ is an additional 'dilation dissipation' term according to a model by Sarkar and Balakrishnan (1990). The turbulent Mach number in this term is defined as

$$M_t = \sqrt{k/a^2}$$

where a is the speed of sound.

The scalar dissipation rate ε is computed by a model transport equation identical to the one used in the standard k–ε model.

Appendix B

The pressure-strain terms (6)

$$\phi_{ij} = \phi_{ij,1} + \phi_{ij,2} + \phi_{ij}^w$$

in Equation 4 are modeled according to Gibson and Launder (1978), Fu et al. (1987) and Launder (1989a, b).

The slow pressure-strain, $\phi_{ij,1}$, is modeled as

$$\phi_{ij,1} = -C_1\rho\frac{\varepsilon}{k}\left[\overline{u_i'u_j'} - \frac{2}{3}\delta_{ij}k\right]$$

with $C_1 = 1.8$.

The rapid pressure-strain term, $\phi_{ij,2}$, is modeled as

$$\phi_{ij,2} = -C_2\left[(P_{ij} + F_{ij} + G_{ij} - C_{ij}) - \frac{2}{3}\delta_{ij}(P + G - C)\right]$$

where $C_2 = 0.60$, P_{ij}, F_{ij} and G_{ij} are defined as in Appendix A

$$C_{ij} = \frac{\partial}{\partial x_k}(\rho u_k\overline{u_i'u_j'}), \quad P = \frac{1}{2}P_{kk}, \quad G = \frac{1}{2}G_{kk} \quad \text{and}$$

$$C = \frac{1}{2}C_{kk}$$

The wall-reflection term, ϕ_{ij}^w, is responsible for the redistribution of normal stresses near the wall. It tends to damp the normal stress perpendicular to the wall, while enhancing the stresses parallel to the wall. This term is modeled as

$$\begin{aligned}\phi_{ij}^w \equiv C_1'\frac{\varepsilon}{k}(&\overline{u_k'u_m'}n_kn_m\delta_{ij} - \frac{3}{2}\overline{u_i'u_k'}n_jn_k - \frac{3}{2}\overline{u_j'u_k'}n_in_k)\\ &\times\frac{k^{3/2}}{C_\ell\varepsilon d} + C_2'(\phi_{km,2}n_kn_m\delta_{ij} - \frac{3}{2}\phi_{ik,2}n_jn_k\\ &- \frac{3}{2}\phi_{jk,2}n_in_k)\frac{k^{3/2}}{C_\ell\varepsilon d}\end{aligned}$$

where $C_1' = 0.5$, $C_2' = 0.3$ n_k is the x_k component of the unit normal to the wall, d is the normal distance to the wall, and $C_\ell = C_\mu^{3/4}/\kappa$ where $C_\mu = 0.09$ and $\kappa = 0.41$.